Organic−Inorganic Hybrid Hollow Nanospheres with Microwindows on the Shell

Jian Liu,[†,‡] Qihua Yang,*[,†] Lei Zhang,[†] Hengquan Yang,[†] Jinsuo Gao,[†,‡] and Can Li*[,†]

State Key Laboratory of Catalysis, Dalian Institute of Chemical Physics, Chinese Academy of Sciences, 457 Zhongshan Road, Dalian 116023, China, and Graduate School of the Chinese Academy of Sciences, Beijing 100039, China

Received January 20, 2008. Revised Manuscript Received March 30, 2008

We demonstrate, for the first time, that organic−inorganic hybrid hollow nanospheres with controllable size (12−20 nm) and shell thickness (4−7 nm) can be successfully synthesized through the condensation of 1,2-bis(trimethoxysilyl)ethane (BTME) around an inorganic-electrolyte-stabilized F127 micelle under a mild buffer condition (NaH_2PO_4−Na_2HPO_4, pH ∼7.0). The hollow spheres feature microwindows with pore size about 0.5−1.2 nm on the shell, which allow the guest molecules to diffuse into the hollow cavities. It was found that the concentration of the buffer solution in the synthesis was crucial to the formation of hollow nanosphere. At a low buffer concentration (20−100 mM), the surfactant exists as individual micelle. A core/shell nanocomposite was formed by the deposition of BTME at the corona of individual micelle, which leads to the formation of organic−inorganic hybrid nanoparticles with hollow interior after the extraction of the surfactant. The aggregation of individual micelles was observed at higher buffer concentration (>200 mM), which favors the formation of irregularly shaped particles with ordered mesostructure. This work presents a novel and facile strategy to fabricate hollow nanospheres with microwindows, which provides a versatile platform for practical applications of organic−inorganic hybrid materials in a broad range of fields such as catalysis, encapsulation, and drug delivery, etc.

Introduction

Hybrid materials with organic and inorganic building blocks uniformly distributed in the framework are particularly attractive because they combine the functional versatility of organic chemistry with the advantages of thermal stability of inorganic substrates.[1,2] It is very important to precisely control the topology and morphology of the organic−inorganic hybrid materials in order to promote the desired applications.[2–11] Among the various morphologies reported so far, spheres with hollow interiors are of special interest. Inorganic hollow spheres have attracted intense research interest because of their low density and thermal and mechanical stability.[9,12–17] If organic−inorganic hybrid materials can be made in the

* To whom correspondence should be addressed. E-mail: yangqh@dicp.ac.cn (Q.Y.); canli@dicp.ac.cn (C.L). Tel: 86-411-84379552 (Q.Y.); 86-411-84379070 (C.L.). Fax: 86-411-84694447. Web site: http://www.hmm.dicp.ac.cn; http://www.canli.dicp.ac.cn.

† Dalian Institute of Chemical Physics, Chinese Academy of Sciences.

‡ Graduate School of the Chinese Academy of Sciences.

(1) Shea, K. J.; Loy, D. A. *Chem. Rev.* **1995**, *95*, 1431–1442. Wen, J. Y.; Wilkes, G. I. *Chem. Mater.* **1996**, *8*, 1667–1681. Shea, K. J.; Loy, D. A. *Chem. Mater.* **2001**, *13*, 3306–3319. Sanchez, C.; Soler-Illia, G. J.; de, A. A.; Ribot, F.; Lalot, T.; Mayer, C. R.; Cabuil, V. *Chem. Mater.* **2001**, *13*, 3061–3083. Gomez-Romero, P. *Adv. Mater.* **2001**, *13*, 163–174.

(2) Hoffmann, F.; Cornelius, M.; Morell, J.; Fröba, M. *Angew. Chem., Int. Ed.* **2006**, *45*, 3216–3251. Hatton, B.; Landskron, K.; Whitnall, W.; Perovic, D.; Ozin, G. A. *Acc. Chem. Res.* **2005**, *38*, 305–312. Kapoor, M. P.; Inagaki, S. *Bull. Chem. Soc. Jpn.* **2006**, *79*, 1463–1475. Stein, A. *Adv. Mater.* **2003**, *15*, 763–775. Sayari, A.; Hamoudi, S. *Chem. Mater.* **2001**, *13*, 3151–3168. Fujita, S.; Inagaki, S. *Chem. Mater.* **2008**, *20*, 891–908.

(3) Vallé, K.; Belleville, P.; Pereira, F.; Sanchez, C. *Nat. Mater.* **2006**, *5*, 107–111.

(4) Warren, S. C.; Disalvo, F. J.; Wiesner, U. *Nat. Mater.* **2007**, *6*, 156–161.

(5) Du, J.; Chen, Y. *Angew. Chem., Int. Ed.* **2004**, *43*, 5084–5087. Perkin, K. K.; Turner, J. L.; Wooley, K. L.; Mann, S. *Nano Lett.* **2005**, *5*, 1457–1461.

(6) Zhang, L.; Abbenhuis, H. C. L.; Yang, Q.; Wang, Y.-M.; Magusin, P. C. M. M.; Mezari, B.; van Santen, R. A.; Li, C. *Angew. Chem., Int. Ed.* **2007**, *46*, 5003–5006. Zhang, L.; Yang, Q.; Yang, H.; Liu, J.; Xin, H.; Mezari, B.; Magusin, P. C. M. M.; Abbenhuis, H. C. L.; van Santen, R. A.; Li, C. *J. Mater. Chem.* **2008**, *18*, 450–457.

(7) Notestein, J. M.; Katz, A. *Chem.—Eur. J.* **2006**, *12*, 3954–3965. Yang, H.; Zhang, L.; Zhong, L.; Yang, Q.; Li, C. *Angew. Chem., Int. Ed.* **2007**, *46*, 6861–6865.

(8) Gu, J.; Fan, W.; Shimojima, A.; Okubo, T. *Small* **2007**, *3*, 1740–1744. Lai, C.-Y.; Trewyn, B. G.; Jeftinija, D. M.; Jeftinija, K.; Xu, S.; Jeftinija, S.; Lin, V. S.-Y. *J. Am. Chem. Soc.* **2003**, *125*, 4451–4459. Trewyn, B. G.; Giri, S.; Slowing, I. I.; Lin, V. S.-Y. *Chem. Commun.* **2007**, 3236–3245. Fowler, C. E.; Khushalani, D.; Lebeau, B.; Mann, S. *Adv. Mater.* **2001**, *13*, 649–652. Rieter, W. J.; Kim, J. S.; Taylor, K. M. L.; An, H.; Lin, W.; Tarrant, T.; Lin, W. *Angew. Chem., Int. Ed.* **2007**, *46*, 3680–3682.

(9) Im, S. H.; Jeong, U.; Xia, Y. *Nat. Mater.* **2005**, *4*, 671–675. Caruso, F. *Adv. Mater.* **2001**, *13*, 11–22. Caruso, F. *Chem.—Eur. J.* **2000**, *6*, 413–419. Caruso, F.; Caruso, R. A.; Möhwald, H. *Science* **1998**, *282*, 1111–1114. Johnston, A. P. R.; Cortez, C.; Angelatos, A. S.; Caruso, F. *Curr. Opin. Colloid Interface Sci.* **2006**, *11*, 203–209.

(10) Djojoputro, H.; Zhou, X. F.; Qiao, S. Z.; Wang, L. Z.; Yu, C. Z.; Lu, G. Q. *J. Am. Chem. Soc.* **2006**, *128*, 6320–6321.

(11) Zhou, X. F.; Qiao, S. Z.; Hao, N.; Wang, X. L.; Yu, C. Z.; Wang, L. Z.; Zhao, D. Y.; Lu, G. Q. *Chem. Mater.* **2007**, *19*, 1870–1876. Tan, B.; Vyas, S. M.; Lehmler, H.-J.; Knutson, B. L.; Rankin, S. E. *Adv. Funct. Mater.* **2007**, *17*, 2500–2508.

(12) Khanal, A.; Inoue, Y.; Yada, M.; Nakashima, K. *J. Am. Chem. Soc.* **2007**, *129*, 1534–1535. Dhas, N. A.; Suslick, K. S. *J. Am. Chem. Soc.* **2005**, *127*, 2368–2369.

(13) Schacht, S.; Huo, Q.; Voigt-Martin, I. G.; Stucky, G. D.; Schüth, F. *Science* **1996**, *273*, 768–771. Liu, J.; Li, C.; Yang, Q.; Yang, J.; Li, C. *Langmuir* **2007**, *23*, 7255–7262. Tan, B.; Lehmler, H.-J.; Vyas, S. M.; Knutson, B. L.; Rankin, S. E. *Adv. Mater.* **2005**, *17*, 2368–2371.

(14) Wang, Q.; Liu, Y.; Yan, H. *Chem. Commun.* **2007**, 2339–2341. Darbandi, M.; Thomann, R.; Nann, T. *Chem. Mater.* **2007**, *19*, 1700–1703.

10.1021/cm800192f CCC: $40.75
Published on Web 06/11/2008

hollow sphere form, a new class of high-performance and highly functional organic−inorganic composites may be achieved.[9] Integration of organic moieties into the framework will modify the surface properties of the materials and meanwhile should also endow the hollow silica nanospheres different physical and mechanical properties. Moreover, the introduction of organic moieties within the silicate network may further tailor the functionality of the hollow nanospheres. These hollow nanospheres embody the advantages of organic−inorganic materials, nanoscale devices, and hollow structures and permit the accommodation of one maximum of elementary functions in a small entity, which will widen the application range of hollow nanospheres and allow the manipulation of the surface properties to control the interactions with various guest species. They are promising candidates for the applications including confined nanocatalysis, bioimaging and biolabeling, artificial cells, controlled-release delivery of drugs, genes, or even proteins.[7,8,11–17] One of the important prerequisites of hollow sphere for practical application is the presence of open channels/windows on the shells, as pathways for the guest species to diffuse into/out of the hollow cavities. For some special applications, such as drug delivery, hollow particles with nanometer size are preferable because such nanoscale particles could be selectively accumulated by tissue because of the enhanced permeability and retention.[8,11–15] However, the design and synthesis of organic−inorganic hybrid hollow spheres with nanometer size and shell windows have remained a challenge. As far as we know, there are no reports on the synthesis of organic−inorganic hybrid hollow spheres with particle sizes less than 50 nm and microwindows on the shell.

Herein, we report for the first time the synthesis of organic−inorganic hybrid hollow nanospheres with built-in functionality and controllable particle size (12−20 nm) in mild NaH_2PO_4−Na_2HPO_4 buffer solution (pH ∼7.0). By assembling 1,2-bis(trimethoxysilyl)ethane (BTME) around the F127 [$EO_{106}PO_{70}EO_{106}$] polymer micelles and subsequent removal of the polymers via ethanol extraction, we synthesized organic−inorganic hybrid hollow nanospheres. More interestingly, the hybrid hollow nanospheres possess microwindows (0.5−1.2 nm) on the shell, which is very important for allowing guest molecules to diffuse into the hollow cavities.

Experimental Section

Chemicals and Reagents. All materials were of analytical grade and used as received without any further purification. Triblock copolymer $EO_{106}PO_{70}EO_{106}$ (F127), ibuprofen drug, and 1,2-bis(trimethoxysilyl)ethane (BTME) were purchased from Sigma-Aldrich Company Ltd. (U.S.A.). Other reagents were obtained from Shanghai Chemical Reagent. Inc., of the Chinese Medicine Group.

Synthesis of the Organic−inorganic Hybrid Hollow Nanosphere. In a typical synthesis, 0.8 g of F127 was dissolved in 28 mL of NaH_2PO_4−Na_2HPO_4 buffer solution (pH ∼7.0, 0.020 mol/L NaH_2PO_4, 0.020 mol/L Na_2HPO_4) at 20 °C under vigorous stirring. When the copolymer was fully dissolved, 2.70 g (10 mmol) of BTME was added to the above solution under stirring. The molar composition of the mixture was 1:0.0032:0.028:0.028:77.8 Si:F127: NaH_2PO_4:Na_2HPO_4:H_2O. The resultant mixture was stirred at 20 °C for 24 h and aged at 100 °C under static conditions for an additional 24 h. The solid product was recovered by filtration and air-dried at room temperature overnight. Finally, the surfactant was extracted by refluxing 1.0 g of the as-synthesized material in 200 mL of ethanol containing 1.5 g of concentrated HCl aqueous solution for 24 h. The powder products were denoted as Et*n*, where *n* refers to the concentration of the buffer solution in mM.

Characterization. X-ray diffraction (XRD) patterns were recorded on a Rigaku RINT D/Max-2500 powder diffraction system using Cu Kα radiation of 0.15406 nm wavelength. The nitrogen sorption experiments were performed at 77 K on a Quantachrome Autosorb-1 system with micropore analysis. Prior to the measurement, the samples were outgassed at 120 °C for at least 6 h. The Brunauer−Emmett−Teller (BET) specific surface areas were calculated using adsorption data at a relative pressure range of P/P_0 = 0.05−0.25. Pore size distributions were derived from the adsorption branch using Barrett−Joyner−Halenda (BJH) method. The microporosity of the hollow nanosphere was calculated using the HK method. The total pore volumes were estimated from the amounts adsorbed at a relative pressure (P/P_0) of 0.99. Transmission electron microscopy (TEM) was performed using a JEOL JEM-2000EX and a FEI Tecnai G^2 Spirit at an acceleration voltage of 120 kV. High-resolution transmission electron microscopy (HR-TEM) images were obtained on a FEI Tecnai G^2 F30 S-Twin. Scanning electron microscopy (SEM) was undertaken on a FEI Quanta 200F scanning electron microscope operating at an accelerating voltage of 1−30 kV. High-resolution scanning electron microscopy (HRSEM) was undertaken on a HITACHI S-4800 scanning electron microscope operating at an accelerating voltage of 20−30 kV. ^{129}Xe NMR spectra were collected at room temperature on a Bruker DRX-400 spectrometer operating at 110.6 MHz with a recycle delay of 1 s, 60°, pulse width of 8 ms, and 1000−4000 scans. Prior to adsorption, all samples were degassed typically at 723 K for 10−20 h. Chemical shifts were referenced to a secondary standard of xenon adsorbed in NaY zeolite and the resonance of which was previously referenced to xenon gas at zero pressure using Jameson's equation. ^{13}C (100.5 MHz) cross-polarization magic angle spinning (CP-MAS) and ^{29}Si (79.4 MHz) MAS solid-state NMR experiments were recorded on a Varian infinity-plus 400 spectrometer. Dynamic light scattering (DLS) measurements were performed at 20 °C using a Coulter Company N4 plus laser-scattering particle meter (detection range: 3−3000 nm). The thermogravimetric analysis (TGA) was performed on a Perkin-Elmer Pyris Diamond TG instrument at a heating rate of 10 °C min^{-1} under a flow of air. FT-IR spectra were collected with a Nicolet Nexus 470 IR spectrometer with KBr pallet.

Adsorption of Probe Molecules. Ibuprofen, BINOL, and Co(Salen) are chosen as the probe molecules to estimate the size of the microwindows on the shell of the hollow nanosphere. Their molecular structures are shown in Figure S1 of the Supporting Information. The adsorption of probe molecules from aqueous solution into hollow nanospheres was performed by using batch equilibrium technique. Typically, 0.2 g of hollow nanospheres was introduced into glass tubes containing 4 mL of probe molecules solution with initial concentrations of 40 mg mL^{-1}. These tubes were transferred into a shaker and shaken for 24 h in order to reach

(15) Huo, Q.; Liu, J.; Wang, L.-Q.; Jiang, Y.; Lambert, T. N.; Fang, E. *J. Am. Chem. Soc.* **2006**, *128*, 6447–6453.
(16) Tang, J.; Zhou, X.; Zhao, D.; Lu, G. Q.; Zou, J.; Yu, C. *J. Am. Chem. Soc.* **2007**, *129*, 9044–9048.
(17) Yuan, J. J.; Mykhaylyk, O. O.; Ryan, A. J.; Armes, S. P. *J. Am. Chem. Soc.* **2007**, *129*, 1717–1723. O'Reilly, R. K.; Joralemon, M. J.; Hawker, C. J.; Wooley, K. L. *Chem. Mater.* **2005**, *17*, 5976–5988.

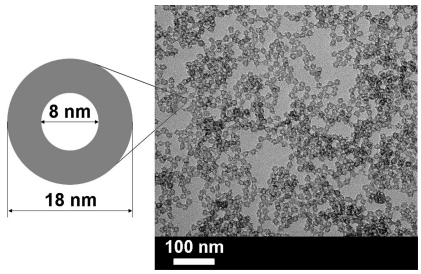

Figure 1. TEM image of the organic−inorganic hollow nanospheres (Et40) synthesized in 40 mM NaH_2PO_4−Na_2HPO_4 buffer solution at an initial temperature of 20 °C and hydrothermal temperature of 100 °C.

the adsorption equilibrium at 25 °C. Upon equilibration, the solid products were recovered by centrifugation. The recovered solid products were subjected to nitrogen sorption analysis.

Results and Discussion

The transmission electron microscopy (TEM) image of a typical sample Et40 (Et*n*, $n = 40$ refers to the concentration of the buffer solution in mM) clearly shows the hollow spherical morphology (Figure 1). Spheres in nanometer size could be clearly observed in the high-resolution scanning electron microscopy (HRSEM) image of this sample (Figure 2). On the basis of the TEM image, we estimated the average particle size of the hollow nanospheres to be around 18 nm, and the average diameter of the hollow core was ca. 8 nm with a shell thickness of ca. 5 nm.

It is interesting to note that a sharp diffraction peak appears at 2θ around 1.0° in the XRD pattern of Et40, which has a spacing of 11.8 nm between the lattice planes (Figure 3). TEM image of Et40 (measured using the powder sample without dispersion in ethanol) shows the existence of wormlike mesopore throughout the sample (see the Supporting Information, Figure S2). Previously, Yokoi et al. reported that the ordered mesoporous structure can be formed by closely packed nanospheres.[18] Moreover, Yu and coworkers described the assembly of the highly ordered mesoporous structure by the hard-spheres packing method.[16] Therefore, the small-angle XRD peak is due to the short-range periodicity of the closely packed nanospheres, which further confirms the results of TEM and SEM that the particle size distribution of the hollow nanospheres is very uniform.

The textural properties of the organic−inorganic hybrid hollow nanospheres were analyzed by N_2 adsorption−desorption isotherms (Figure 4). Et40 shows typical type IV isotherms of mesoporous materials. It is noteworthy that there are two capillary condensation steps in the adsorption isotherm, suggesting that this sample has two types of mesopores. The pore size distribution curve shows that the primary and secondary mesopore diameters are 6.5 and 29 nm, respectively (Figure 4). The primary pore can be ascribed to the inner void of the hollow nanospheres, and the secondary mesopore corresponds to the interparticle void formed from the packing of the nanospheres.[16,19,20] The slight difference in the core size determined from the TEM image and N_2 sorption characterization may be due to the fact that the BJH model was not very suitable for measuring the sizes of cage-like pores.[11] Et40 has specific surface area as high as 1011 $m^2\ g^{-1}$ and large pore volume of 2.74 $cm^3\ g^{-1}$ (see the Supporting Information, Table S1).

The compositional information of the organic−inorganic hybrid hollow nanospheres was collected with FT-IR and solid-state NMR techniques. IR spectrum of the extracted sample shows bands at 1272, 1412, 2890, and 2895 cm^{-1}, which can be assigned to C−H vibrations of the bridging ethylene group (see the Supporting Information, Figure S3). After the extraction step, the bands at 1350, 1376, 1463, 2907, and 2076 cm^{-1} corresponding to F127 disappear, suggesting that the surfactant is almost completely removed by extraction. The weak adsorption band at 2980 cm^{-1} is due to the ethoxy groups formed during the surfactant extraction process. Figure S4 of the Supporting Information shows the ^{13}C CP-MAS NMR and ^{29}Si MAS NMR spectra of Et40. A resonance band at 6.3 ppm confirms the ethylene groups incorporated in the materials. The peaks centered at 58.0 and 16.2 ppm are due to the carbons of the ethoxy groups formed during the surfactant extraction process, which is consistent with the FT-IR results. ^{29}Si NMR spectrum of Et40 shows the existence of ^{n}T sites as expected. The sharp signals at −65.2 and −59.2 ppm can be attributed to [^{3}T, $SiC(OSi)_3$] and [^{2}T, $(OH)SiC(OSi)_2$] silicon connected with the ethylene groups, respectively.[20] The results of NMR and FT-IR confirm the successful incorporation of ethylene groups into the network, and the almost complete removal of the surfactant by the extraction method.

Figure S5 of the Supporting Information displays the thermogravimery (TG) profiles and the corresponding differential TG (DTG) patterns for as-synthesized and extracted Et40 recorded in an air atmosphere. The TG curve of the as-synthesized Et40 features a four-step weight loss behavior with the treatment temperature from 25 to 900 °C. The weight loss (ca. 2 wt %) below 120 °C is due to the adsorbed water and ethanol. Further increasing the temperature, three distinct weight loss steps proceeded from 160 to 220 °C, 230 to 550 °C, and 550 to 700 °C, respectively. The second weight loss step that occurs in the range of 160−220 °C with relatively large weight loss (ca. 20 wt %) can be attributed to the decomposition of block copolymer. This is followed by a weight loss extended to 550 °C, which can be ascribed to the decomposition of the bridging ethylene groups and block copolymer residues. The last weight loss beyond 550 °C arises from the decomposition of organic residues groups and the condensation of silanols.[20] In contrast, the absence of the characteristic peak for the F127 polymer template on the DTG patterns of the extracted Et40 reflects almost complete removal of the polymer. The decomposition of the bridging ethylene groups starts at 230 °C, indicating that the hybrid hollow nanospheres are thermally stable below this temperature.

(18) Yokoi, T.; Sakamoto, Y.; Terasaki, O.; Kubota, Y.; Okubo, T.; Tatsumi, T. *J. Am. Chem. Soc.* **2006**, *128*, 13664–13665.
(19) Suzuki, K.; Ikari, K.; Imai, H. *J. Am. Chem. Soc.* **2004**, *126*, 462–463. Oaki, Y.; Kotachi, A.; Miura, T.; Imai, H. *Adv. Funct. Mater.* **2006**, *16*, 1633–1639.
(20) Yang, Q.; Yang, J.; Liu, J.; Li, Y.; Li, C. *Chem. Mater.* **2005**, *17*, 3019–3024. Liu, J.; Yang, Q.; Zhang, L.; Jiang, D.; Shi, X.; Yang, J.; Zhong, H.; Li, C. *Adv. Funct. Mater.* **2007**, *17*, 569–576. Zhang, L.; Liu, J.; Yang, J.; Yang, Q.; Li, C. *Microporous Mesoporous Mater.* **2008**, *109*, 172–183.

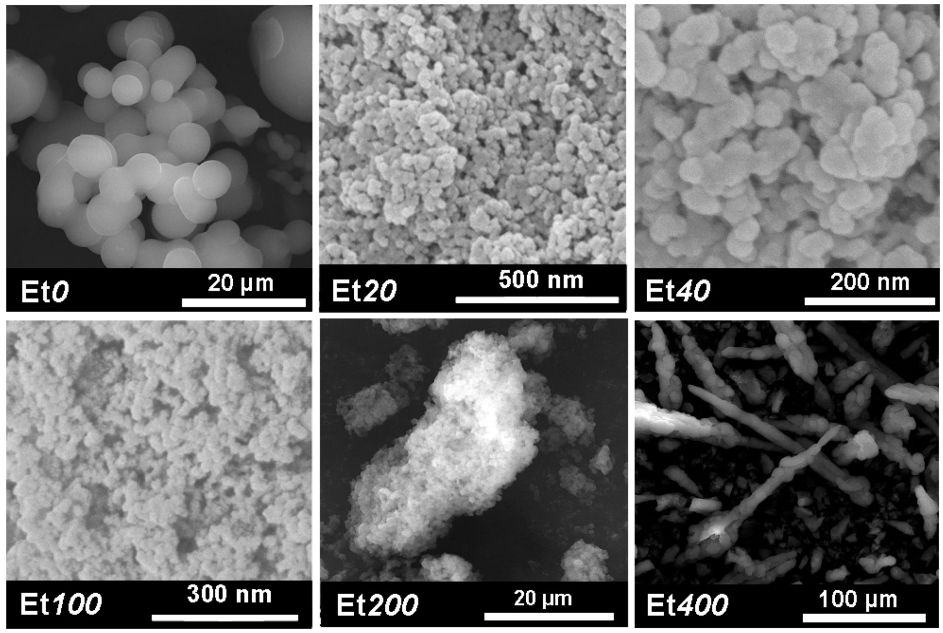

Figure 2. SEM images of the organic−inorganic hybrid hollow nanospheres synthesized with different buffer solution concentrations at an initial temperature of 20 °C and hydrothermal temperature of 100 °C.

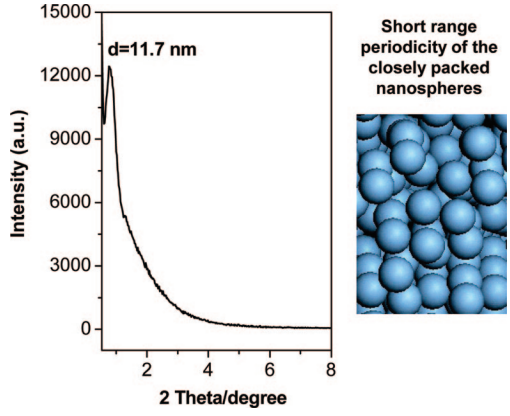

Figure 3. XRD patterns of the organic−inorganic hollow nanospheres synthesized in 40 mM NaH_2PO_4−Na_2HPO_4 buffer solution at an initial temperature of 20 °C and hydrothermal temperature of 100 °C.

The porosity of the hybrid hollow nanospheres (Et40) was further investigated using the hyperpolarized ^{129}Xe NMR technique because the chemical shift of xenon highly depends on the pore size of the porous materials.[21,22] ^{129}Xe NMR clearly shows the void pores of the organic−inorganic hollow nanosphere. The sorption of ^{129}Xe atom in the hollow of the materials directly again indicates the presence of windows on the shell (Supporting Information, Figure S6). In addition to the mesoporosity, HK pore size distribution clearly shows that Et*40* has micropores with diameter in the range of 0.5−1.2 nm on the shell (Figure 4). HRTEM images of Et40 also suggest the presence of the micropores (<1 nm) on the shell of the hollow nanosphere, which are randomly interconnected to reach the inner cavity (see the Supporting Information, Figure S7).

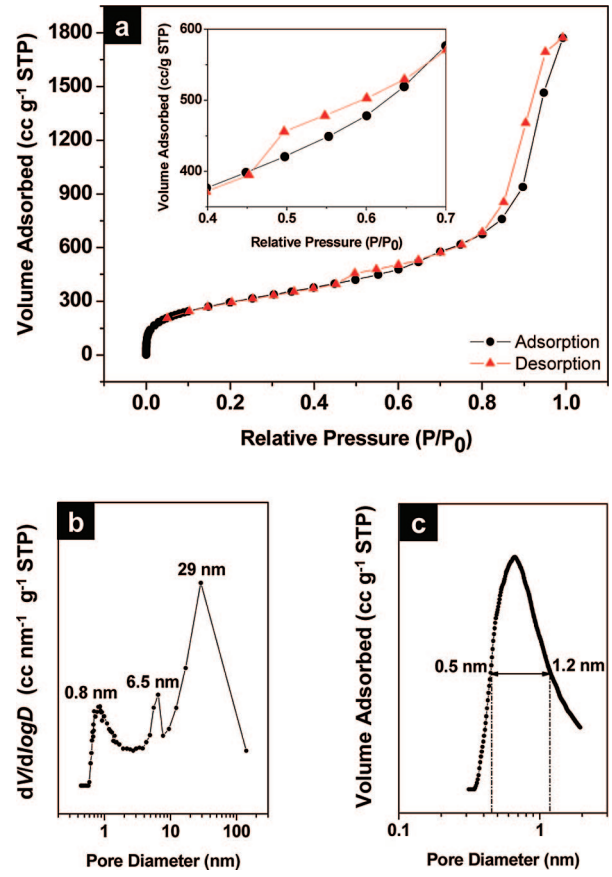

Figure 4. (a) Nitrogen adsorption (●) and desorption (▲) isotherm (inset is the enlarged part of isotherm at P/P_0 from 0.4 to 0.7); (b) BJH pore size distribution curve; and (c) HK pore size distribution curve of organic−inorganic hollow nanospheres (Et40).

The existence of a micropore well-connected to the hollow interior provides the opportunity for the adsorption of gust molecules into the hollow nanospheres. The adsorption capacity of Et40 for guest molecules with different molecular

(21) Bonardet, J.-L.; Fraissard, J.; Gédéon, A.; Springuel-Huet, M.-A. *Catal. Rev.—Sci. Eng.* **1999**, *41*, 115–225.
(22) Chen, F.; Zhang, M.; Han, Y.; Xiao, F.; Yue, Y.; Ye, C.; Deng, F. *J. Phys. Chem. B* **2004**, *108*, 3728–3734.

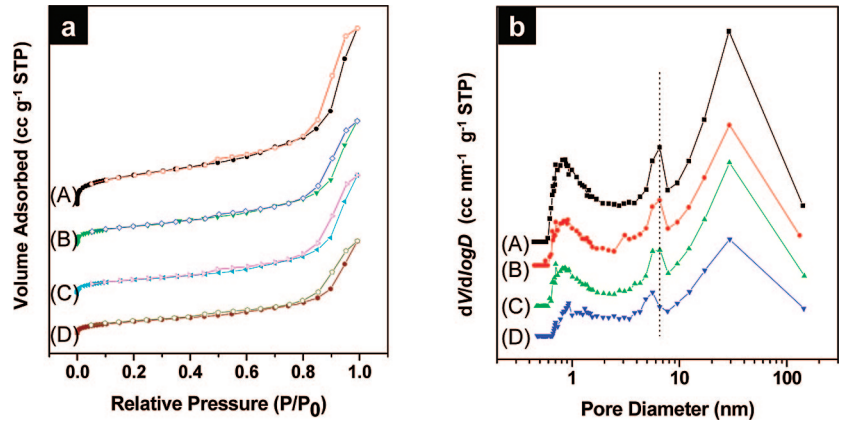

Figure 5. (a) Nitrogen adsorption (●) and desorption (○) isotherms and (b) pore size distribution curves of organic−inorganic hollow nanospheres (Et40) before and after adsorption of probe molecules. (A) Et40; (B) Co(Salen)/Et40; (C) BINOL/Et40; (D) ibuprofen/Et40.

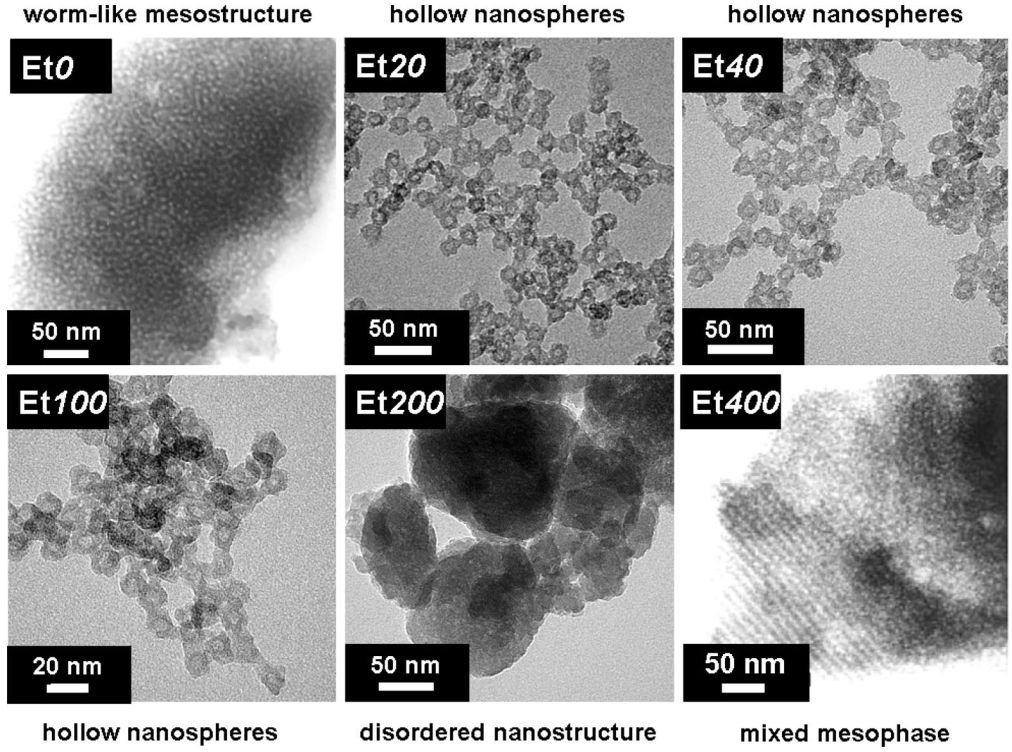

Figure 6. TEM images of the organic−inorganic hybrid materials: synthesized with different concentrations of buffer solution at an initial temperature of 20 °C and hydrothermal temperature of 100 °C.

size was performed, i.e., ibuprofen (0.52 × 1.02 nm^2), BINOL (0.70 × 0.97 nm^2) and Co(Salen) (1.20 × 1.80 nm^2) (see the Supporting Information, Figure S1). After adsorption with the probe molecules, the shape of the N_2 sorption isotherm of Et40 was unchanged (Figure 5), whereas the BET surface area, pore volume, and micropore volume of Et40 decreased sharply (see the Supporting Information, Table S1). When ibuprofen and BINOL were used as the probe molecules, the primary pore diameter (the hollow core) was decreased from 6.5 to 5.5 and 6.1 nm, respectively. These results suggest that the pore diameter on the shell is larger than or close to the molecular size of ibuprofen and BINOL and allows the diffusion of the probe molecules into the interior of the hollow nanospheres. When Co(Salen) was used as the probe molecule, the primary pore diameter remained almost the same, implying that the pore diameter on the shell is smaller than the molecular size of Co(Salen) (1.20 × 1.80 nm^2). The differences in the pore filling effectiveness of the probe molecules suggest that the pore diameter on the shell of the hollow sphere is ca. 0.5−1.2 nm. The presence of porosity on the shell of the hollow spheres is very important for their applications. Above results further confirm the existence of microwindows on the shell of the hollow nanospheres.

To gain further insights into the formation mechanism of the organic−inorganic hybrid hollow nanospheres, we synthesized a series of organic−inorganic hybrid materials in NaH_2PO_4−Na_2HPO_4 buffer solutions with different concentrations (0, 20, 40, 100, 200, and 400 mM). TEM images of the hybrid organic−inorganic materials synthesized at different buffer concentrations are shown in Figure 6. Et0 synthesized in the absence of inorganic salts has wormlike mesoporous structure and spherical morphology with average

particle size of 6 μm (Figures 2 and 6 and the Supporting Information, Figure S8). The hollow nanospheres with particle size of 18 nm were clearly observed in the TEM images of sample Et20, Et40, and Et100 (Figure 6). The HRSEM images of these samples show the closely packed nanospheres, further confirming that these samples have the nanosphere morphology (Figure 2). TEM and SEM images reveal that the hollow nanospheres are very uniform. Et100 consists of more aggregated nanoparticles compared with other Et*n* (n = 20, 40) samples. Disordered structure was observed in the TEM image of Et200 (Figure 6). The SEM image of Et200 shows aggregated silica spheres (~600 nm) with grapelike morphology (Figure 2). Further increasing the buffer concentration to 400 mM, Et400 exhibits the mixed phase of ordered pore arrangement (*Im*3*m*) and wormlike structure (Figure 6 and the Supporting Information, Figure S8). The SEM image shows that this sample has stalactite-like morphology (Figure 2). Thus, by changing the buffer concentration from 0 to 400 mM, the organic−inorganic hybrid materials gradually evolve from the wormlike mesostructure to hollow nanosphere then to the mixed phase. The concentrations of the buffer solution have a great impact on the mesostructure and morphology of the organic−inorganic hybrid materials. The hybrid hollow nanosphere can be synthesized by controlling the buffer concentrations in the range of 20−100 mM.

The micelle structure formed during the synthesis is sensitive to the concentration of inorganic electrolyte.[23,24] The dynamic light scattering (DLS) measurement was employed to measure the micelle diameter of F127 in the solution at different buffer concentrations (see the Supporting Information, Figure S9). Without sodium phosphate in the synthesis medium, the dynamic diameter of F127 micelle was measured to be 3 nm, and only wormlike mesostructure was formed because of the weak interaction between the surfactant micelle and hydrolyzed organosilica species under neutral conditions.[21] The pore diameter of the Et0 is 3.9 nm from N_2 sorption analysis, which is consistent with the dynamic micelle diameter of 3 nm. When small amounts of sodium phosphate were added (40 mM buffer solution), the hydrodynamic micelle diameter increases to 18.9 nm (see the Supporting Information, Figure S9), which is in the similar range of the individual micelle diameter.[15] The formation of individual micelle in the presence of small amounts of surfactant is due to the salting-out effect of sodium phosphates, which may decrease the critical micelle concentration (CMC) and critical micelle temperature (CMT).

Light scattering studies show that the presence of small amounts of sodium phosphate is beneficial for the formation of individual surfactant micelles. When BTME is added to the synthesis solution, it penetrates into the micelle core and then condenses around the PEO chain of the individual micelle. The hydrodynamic diameter of the F127 surfactant micelle is correlated well with the particle size observed from TEM image, further confirming that BTME is condensed around the PEO chain of the individual micelle. The hydrodynamic micelle diameter of F127 is increased to about 75 nm when the buffer concentration is increased to 400 mM (see the Supporting Information, Figure S9), indicating the aggregation of the individual micelles. The existence of large amounts of sodium phosphate can increase the micelle microviscosity and induce the aggregation of micelles.[15,25–28] The coassembly of the hydrolyzed organosilicas around the surfactant micelles results in the formation of nanoporous structure (the mixed phase of wormlike structure and ordered *Im*3*m* phase). The formation of the microwindows on the shell is related to the hydrophilic nature of EO-blocks of F127 polymer. The PEO can penetrate into the organosilicate layer during the assembly process, which results in micropore on the shell of the hollow nanospheres.[24,29] The results of DLS show that the micelle structure can be tuned by varying the buffer concentration. The behavior of the micelle in the initial solution controls the morphology and mesostructure of the resultant organic−inorganic hybrid materials.

The TEM images of the organic−inorganic hybrid materials synthesized at different hydrothermal temperatures are shown in Figure S10 of the Supporting Information. Without hydrothermal treatment, aggregated solid nanosphere was observed in the TEM image. The aggregated hollow nanosphere is formed when the hydrothermal temperature is increased to 80 °C. The formation of monodispersed hollow nanospheres was realized when the hydrothermal temperature was raised to 100−120 °C. The core−shell nanostructure is closer to a thermodynamically favored mesophase formed due to the decreasing of the surface free energy (ΔF). The shrinkage of organosilicate shell and withdrawal of the PPO core of F127 during the hydrothermal process also contribute to the formation of hollow nanosphere. The above results indicate that higher hydrothermal temperature favors the formation of hollow nanospheres.

It is also worth mentioning that hollow nanospheres can be obtained with other salting-out inorganic electrolytes, such as NaAc, Na_2SO_4, and $NaHCO_3$ (Figure 7). In contrast, hollow nanospheres can not be obtained by introducing inorganic electrolytes, such as $NaNO_3$, in the system.[25–27] These results further confirmed the formation mechanism that (1) the single surfactant micelle can be formed at low surfactant concentration with the aid of salting-out inorganic electrolyte, (2) The assembly of the BTME around the single surfactant micelle leads to the formation of organic−inorganic hybrid hollow nanospheres (Scheme 1). Moreover, the size and shell thickness of the hollow spheres could be controlled in the range of 12−20 and 4−7 nm, respectively, through adjusting the BTME:F127 molar ratio in the initial mixture

(23) Alexandridis, P.; Holzwarth, J. F.; Hatton, T. A. *Macromolecules* **1994**, *27*, 2414–2425. Kumbhakar, M.; Goel, T.; Nath, S.; Mukherjee, T.; Pal, H. *J. Phys. Chem. B* **2006**, *110*, 25646–25655.
(24) Wanka, G.; Hoffmann, H.; Ulbricht, W. *Macromolecules* **1994**, *27*, 4145–4159.
(25) Bagshaw, S. A. *Chem. Commun.* **1999**, 1785–1786.
(26) Yu, C.; Tian, B.; Fan, J.; Stucky, G. D.; Zhao, D. *J. Am. Chem. Soc.* **2002**, *124*, 4556–4557.
(27) Leontidis, E. *Curr. Opin. Colloid Interface Sci.* **2002**, *7*, 81–91. Pandit, N.; Trygstad, T.; Croy, S.; Bohorque, M.; Koch, C. *J. Colloid Interface Sci.* **2000**, *222*, 213–220. Desai, P. R.; Jain, N. J.; Sharma, R. K.; Bahadur, P. *Colloids Surf., A* **2001**, *178*, 57–69. Che, S.; Lim, S.; Kaneda, M.; Yoshitake, H.; Terasaki, O.; Tatsumi, T. *J. Am. Chem. Soc.* **2002**, *124*, 13962–13963.
(28) Yu, C.; Fan, J.; Tian, B.; Zhao, D. *Chem. Mater.* **2004**, *16*, 889–898.
(29) Ryoo, R.; Ko, C. H.; Kruk, M.; Antochshuk, V.; Jaroniec, M. *J. Phys. Chem. B* **2000**, *104*, 11465–11471.

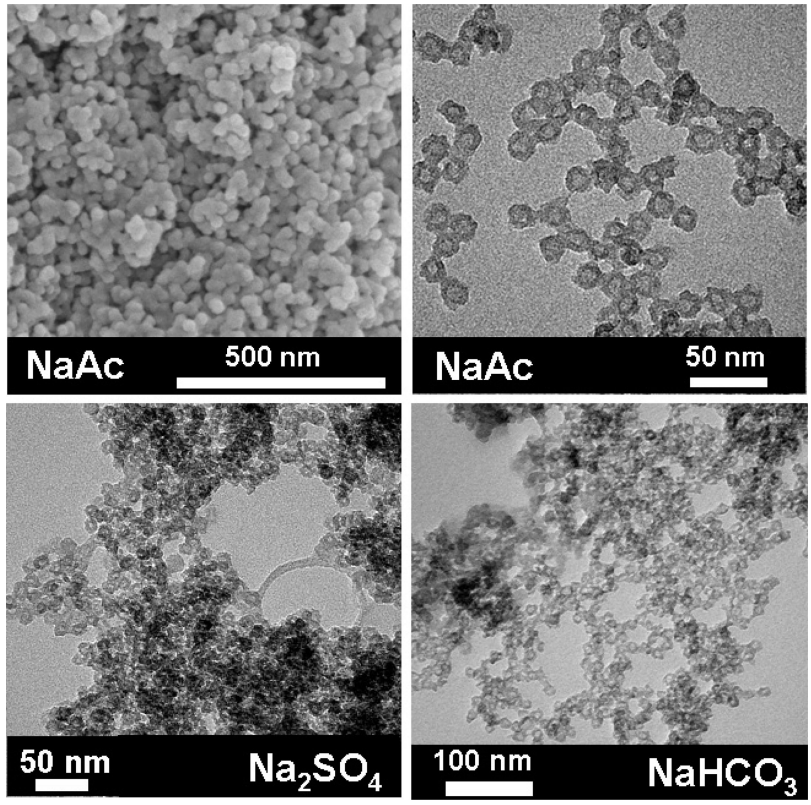

Figure 7. SEM image and TEM images of the organic−inorganic hybrid hollow nanospheres synthesized with different salt solutions at an initial temperature of 20 °C and hydrothermal temperature of 100 °C.

Scheme 1. Schematic Illustration of the Formation of Organic−Inorganic Hybrid Hollow Nanospheres

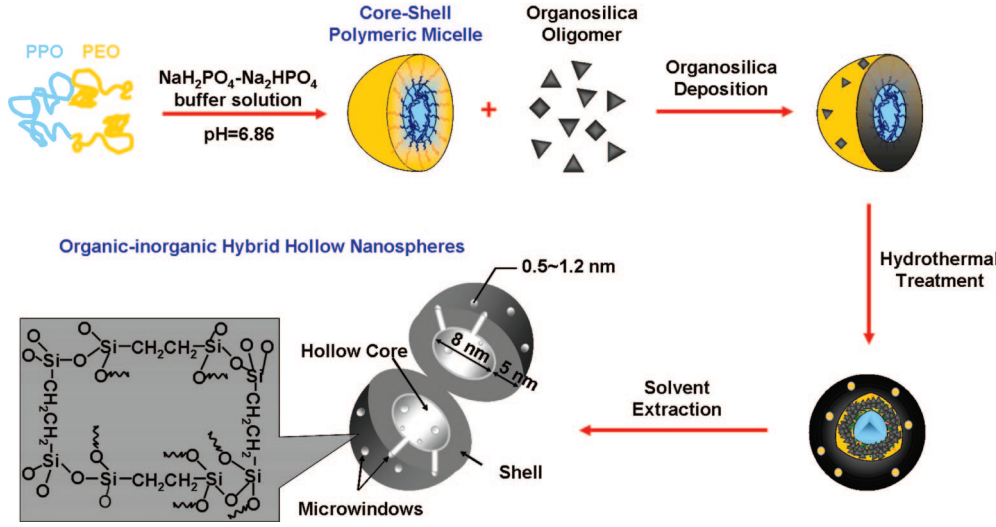

(see the Supporting Information, Figure S11). For comparison, we also tried to synthesize the hollow nanosphere using tetraethoxysilane (TEOS) or tetramethoxysilane (TMOS) as silane precursors under the current synthetic conditions. Using TEOS as the silane precursor, the formation of silica hollow microspheres (0.5−8 μm) was observed. The highly aggregated silica hollow nanospheres with diameter about 12 nm could be obtained with TMOS as the silane precursor.

Conclusions

In summary, the organic−inorganic hybrid hollow nanospheres with controllable size (12−20 nm) and shell thickness (4−7 nm) were synthesized by assembling BTME around block copolymer F127 micelles in NaH_2PO_4−Na_2HPO_4 buffer solution. With buffer concentration in the range of 20−100 mM, BTME was selectively deposited at the corona of individual micelles, resulting in the formation of the organic−inorganic hybrid nanoparticles with well-defined core−shell morphologies. Moreover, there are extensive microwindows (0.5−1.2 nm) on the shell of the hollow sphere, which can allow the diffusion of guest molecules into/out of the interior. The hollow nanospheres with uniform particle size can be assembled in short-range periodicity. Our approach is applicable to a wide range of

compositions. Combining the advantages of hybrid materials and hollow structures, the organic−inorganic hybrid hollow nanospheres with microwindows on the shell open the opportunity to a broad range of interests such as catalysis, encapsulation, and drug delivery.

Acknowledgment. We thank the National Natural Science Foundation of China (20321302, 20503028, 20621063, 20673113) and the National Basic Research Program of China (2003CB615803, 2005CB221407) for financial support. We thank Prof. Mengfei Luo for HRSEM images, Mr. Xuming Wei and Prof. Dangsheng Su for HRTEM images and helpful discussion, and Mr. Yong Liu and Dr. Weiping Zhang for the hyperpolarized ^{129}Xe NMR measurements. We are grateful to Prof. Dongyuan Zhao from Fudan University and Prof. Qisheng Huo from Jilin University for fruitful discussion.

Note Added after ASAP Publication. In the version of this paper published to the Web on June 11, 2008, the ^{129}Xe experimental parameters were incorrect. The corrected version was published July 1, 2008.

Supporting Information Available: Hyperpolarized ^{129}Xe NMR, ^{13}C CP-MAS NMR and ^{29}Si MAS NMR, dynamic light scattering (DLS), HRTEM, FTIR, TG/DTG characterizations of organic−inorganic hybrid hollow nanosphere (PDF). This material is available free of charge via the Internet at http://pubs.acs.org.

CM800192F